LAWRENCE
LIVERMORE
NATIONAL
LABORATORY

LLNL-TR-515275

Dual and Triple Ion-Beam Irradiations of Fe, Fe(Cr) and Fe(Cr)-ODS Final Report: IAEA SMoRE CRP

M. J. Fluss, L. L. Hsiung, J. Marian

November 21, 2011

Disclaimer

This work performed under the auspices of the U.S. Department of Energy by Lawrence Livermore National Laboratory under Contract DE-AC52-07NA27344.

Dual and Triple Ion-Beam Irradiations of Fe, Fe(Cr) and Fe(Cr)-ODS Final Report: IAEA SMoRE CRP[#]

November 2011

Michael J. Fluss, Chief Scientific Investigator
Michael J. Fluss, Luke L. Hsiung and Jaime Marian, Authors

Lawrence Livermore National Laboratory
Livermore, California 94550 USA

1 Abstract

Structures of nanoparticles in Fe-16Cr-4.5Al-0.3Ti-2W-0.37Y2O3 (K3) and Fe-20Cr-4.5Al-0.34Ti-0.5Y2O3 (MA956) oxide dispersion strengthened (ODS) ferritic steels produced by mechanical alloying (MA) and followed by hot extrusion have been studied using high-resolution transmission electron microscopy (HRTEM) techniques to to gain insight about the formation mechanism of nanoparticles in MA/ODS steels. The observations of Y-Al-O complex-oxide nanoparticles in both ODS steels imply that decomposition of Y2O3 in association with internal oxidation of Al occurred during mechanical alloying. While the majority of oxide nanoparticles formed in both steels is Y4Al2O9, a few oxide particles of YAlO3 are also occasionally observed. These results reveal that Ti (0.3 wt %) plays an insignificant role in forming oxide nanoparticles in the presence of Al (4.5 wt %). HRTEM observations of crystalline nanoparticles larger than ~2 nm and amorphous or disordered cluster domains smaller than ~2 nm provide an insight into the formation mechanism of oxide nanoparticle in MA/ODS steels, which we believe from our observations involves a solid-state amorphous precursor followed by recrystallization. Dual ion-beam irradiations using He^{+}+Fe^{+8} ions were employed to gain more detailed insight about the role of nanoparticles in suppressing radiation-induced swelling. This is elaborated through TEM examinations of cavity distributions in ion-irradiated Fe-14Cr and K3-ODS ferritic steels. HRTEM observations of helium-filled cavities (helium bubbles) preferably trapped at nanoscale oxide particles and clusters in ion-irradiated K3-ODS are presented. Finally, we describe the results from triple ion-beam irradiations using H^{+}+He^{+}+Fe^{+8} ions to emulate fusion first wall radiation effects. Preliminary work is reported that confirms the existence of significant hydrogen synergistic effects described earlier by Tanaka et al., [1] for Fe(Cr) and by Wakai et al., [2, 3] for F82H reduced activation ferritic martensitic (RAF/M) steel. These previous results combined with our data suggest a complex new "catalytic" mechanism whereby H interacts with the steady state population of defects and the embryonic cavities so as to accelerated cavity (void) growth in both Fe(Cr) and under special conditions in ODS steels.

[#] *This work performed in part under the auspices of the U.S. Department of Energy by Lawrence Livermore National Laboratory under Contract DE-AC52-07NA27344.*

2 Rationale for the project

One of the major challenges in designing future fusion reactors is to develop the high-performance structural materials for first wall and breeder blanket, which will be exposed to the displacement damage from fusion neutrons **(**≤14 MeV**)** from the deuterium-tritium fusion, and to the bulk production of helium **(**He**)** and hydrogen **(**H) from the *(n,a), (n,p), and (n,np)* transmutation reactions [4]. The choice of structural materials dictates the design and purpose of the fusion reactor system. As an example consider the sequence of materials choices for ITER, DEMO, and a commercial fusion system. ITER's structural components are standard steels, DEMO will likely utilize RAF/M steels, and while a future fusion commercial plant may use refractory alloys or even ceramics such as SiC/SiC_{fiber}. In particular, the allowable power plant operating temperature, the choice of coolant, and the power conversion system are critically dependent on the performance characteristics of the materials. The selection of suitable structural materials is based on conventional properties **(**such as thermophysical, mechanical, and corrosion and compatibility**)**, low neutron-induced radioactivity, and resistance to radiation-induced damage phenomena such as material hardening/embrittlement and/or dimensional instability caused by void- and helium-driven swelling [4, 5].

Oxide dispersion strengthened **(**ODS**)** steels, which are produced by mechanical alloying **(**MA) of elemental powders or prealloyed metallic powder with yttria **(**Y_2 O_3**)** powder and consolidated by hot extrusion or hot isostatic pressing, are a class of advanced structural materials with a potential to be used at elevated temperatures due to the metallurgical enhancements from the dispersion of thermally stable oxide nanoparticles into the matrix. ODS steels are resistant to radiation-induced swelling and have improved creep strength and oxidation/corrosion resistance at elevated temperatures compared to conventional steels. Thus an operating temperature of the first wall in future fusion reactors of >700 °C [6] is possible, resulting in an improved energy efficiency ≥40% [7].

Although significant progress has been made recently on the processing-microstructure-property relationships of RAF/M and ODS steels [8, 9], it remains to understand the role of fusion-relevant helium and hydrogen transmutation gases on their deformation, fracture, and cavity swelling. Since no prototype fusion reactors currently exist, it is difficult to directly evaluate the effects of high-energy neutron and transmutation gases on the first wall and blanket of a fusion reactor. One technique commonly used to study the evolution of defect structures and the kinetics of cavity formation utilizes transmission electron microscopy (TEM) examinations of specimens simultaneously bombarded by heavy ions and helium and/or hydrogen ions through so-called "dual-beam" and/or "triple-beam" accelerated experiments [1]. The heavy ions create atomic displacements while the implanted gas ions emulate transmutation gases, helium (~10 appm/dpa) and hydrogen (~40–45 appm/dpa) [4, 10].

3 Overview of the initial project plan

While some modifications of the initial project plan were required the overall project proceeded along the lines originally outlined and produced significant new data.

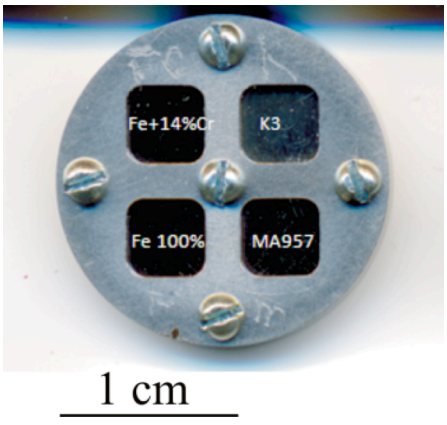

Figure 1 Specimen holder for JANNUS heating stage indicating the types of specimens irradiated in these studies.

3.1 Dual beam irradiation

The ODS steels used for this investigation were Fe-16Cr-4Al-2W-0.3Ti-0.3Y2 O3 _ designated as K3 _ Ref. 9__ ODS ferritic steels and Fe-20Cr-4.5Al-0.34Ti-0.5Y2 O3 _ designated as MA956 _ Ref. 10__ or MA957. A full description of the fabrication procedure for the ODS steels can be found elsewhere.11,12 For the purpose of investigating the role of nanoparticles in radiation tolerance of ODS steels, a non-ODS Fe-14 wt % Cr alloy was also prepared using a vacuum arc-melting method followed by hot rolling at 1050 °C. Dual-beam irradiation of Fe-14Cr alloy and K3-ODS steel loaded in a stainless-steel specimen holder using 24 MeV Fe^{+8} ions for displacement damage and energy-degraded 1.7 MeV He^{+} ions for helium implantation was conducted at the JANNUS facility, Saclay, France. The irradiation temperature was controlled at 425±5°C using a proportional-integral-derivative referenced thermocouple located on the specimen holder (Figure 1). The specimen temperature uniformity was estimated by monitoring the surface temperature of the specimen using a digital infrared camera during heating and ion irradiation. The surface temperature was uniform within ~2.5 °C and tracked well with the controlling thermocouple. The displacement damage in dpa (displacement per atom) from Fe^{8+} as a function of depth into the specimen, and the He^{+} implantation profile were deduced using the SRIM code [11]. The implantation depth of helium was over a region extending from 1.5 to 2.6 μm beneath the specimen surface to avoid overlapping with the Fe^{8+} ion implanted region that extended from 2.75 to 3.6 μm beneath the specimen surface. The displacement damage at the peak position was 65 dpa and the specimens were irradiated in the region under test at ~$5*10^{-4}$ dpa/s. The nominal time integrated radiation conditions for the volume under test are as follows: the displacement damage increases from 10 dpa at 1.5 μm to 40 dpa at 2.75 μm, and there are two peaks for the helium implantation (100 appm/dpa at 2.1 μm and 25 appm/dpa at 2.6 μm) that defined the volume under test. Most of the analyses was done in the region associated with the larger He peak. The dose parameters were 80 appm He/dpa, and an average of 40 dpa in the middle of the region under test.

3.2 Triple beam irradiation

A triple beam (H+He+Fe) irradiation was performed on four specimens soon after the three-beam facility came on-line at JANNUS-Saclay. The irradiation was conducted at 625°C using the same beam energies and dose rate as for the dual beam irradiation but with the addition of hydrogen (680 keV) such that the hydrogen was implanted in the same volume (depth) as the helium. Again, the volume under test was a region of ~0.5

micron thick from 2.1 to 2.6 microns in depth. The dose parameters were, 40 appm H/dpa, 16 appm He/dpa, and an average of 40 dpa in the middle of the region under test.

3.3 High resolution transmission electron microscopy (HRTEM)

Thin foils of the as fabricated ODS steels for TEM examination were prepared by a standard procedure that includes slicing, grinding, and polishing. Final thinning of the foils was performed using a standard twin-jet electro-polishing technique in an electrolyte (90 vol % acetic acid, 10 vol % perchloric acid) at 30 V and room temperature. Cross-section TEM foils (10 μm x 6 μm x <0.1 μm) of irradiated Fe-14Cr and K3-ODS were prepared using a focused ion-beam method. The foils were lifted out using a micro-pickup system and mounted onto a copper grid. TEM characterizations were performed using a Phillips CM300 field-emission transmission electron microscope (accelerating voltage of 300 kV). A software package, CARINE CRYSTALLOGRAPHY 3.1 [12] was used to simulate electron diffraction patterns to identify the crystal structure of oxide nanoparticles.

4 Modification and deviations from initial plan

The initial project plan was modified to accommodate operational aspects of the multi-ion beam facility at JANNUS-Saclay [13] resulting in carrying out experiments to dose of <40dpa. Additionally, plans to perform micro-mechanical measurements on the irradiated materials were deferred to the future. The irradiated specimens are still available for future post irradiation examination with micro-mechanical techniques as well as 3D atom probe.

5 Collaborations within the project

The successes in this project are the result of the work and contributions of many collaborators. They are listed in Tbl. 1 by institution.

Tbl. 1

Collaborators	Institution
Michael J. Fluss Luke L. Hsiung B. William Choi Scott Tumey Jaime Marian Paul Ehrart Vasily Bulatov	Lawrence Livermore National Laboratory Physical and Life Sciences Directorate Livermore, CA 94566 USA
Yves Serruys Estelle Meslin Francois Willaime	Service de Recherches de Métallurgie Physique, CEA, Gif-sur-Yvette 91191 France
Akihiko Kimura	Institute of Advanced Energy, Kyoto University, Gokasho, Uji, Kyoto 611-0011, Japan

6 Results

6.1 As manufactured TEM characterization of Fe(Cr) alloy and ODS steel

6.1.1 Inclusions in Fe(Cr) alloy

An interesting aspect of the Fe(14at%Cr) alloy used in this study was the revealing of small "impurity" sites upn exposure to the dual beam irradiation. We believe that these sites are present in the as manufactured material but are at the resolution limit of the TEM and hence difficult if not impossible to observe. Figure 2 elaborates this observation by showing the nucleation of helium bubbles in association with dislocation and then at high magnification highlighting the core inclusions at the center of two of the bubbles.

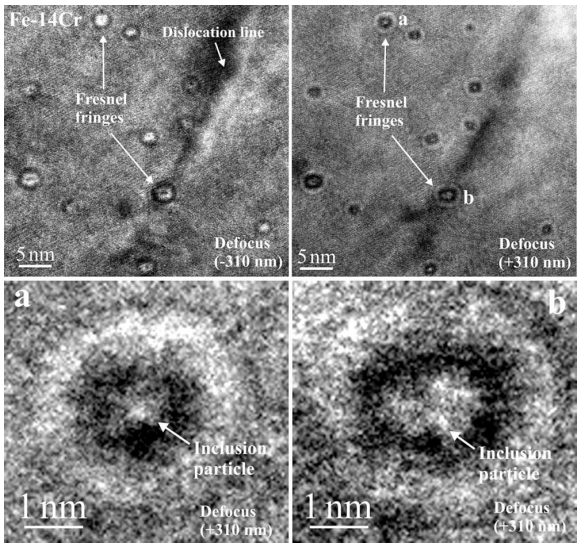

Figure 2 Bright-field TEM images show the heterogeneous nucleation of helium bubbles in association with dislocation lines and inclusion particles. The high-magnification TEM images taken from the bubbles labeled a and b reveal that inclusion particles of _1 and _2 nm can be readily seen within these two bubbles, which appear as black contrasts surrounded by a white Fresnel fringe in overfocus images. *From [14]*

6.1.2 ODS particle morphology and crystallization

The larger (> 1nm) ODS particles crystalize during consolidation and heat treatment of the mechanically alloyed powder. This crystallization process is determined not only by the energetics, but by complex kinetics. We have observed that the precursor to the crystallization, and the formation of the so-called core shell structure, is an amorphous aggregation of the oxide materials. The experimental evidence for this is found in Figure 3 and Figure 4. In Figure 3 we show the presence of an amorphous domain in the midst of a particle that was in the process of crystalizing. This feature was quite common in both the K3 and MA956 specimens investigated. In Figure 4 is the strongest evidence for the existence of an amorphous precursor to crystallization, the formation of multiple domains in the oxide particle, which can only happen if the particle is preceded by an amorphous

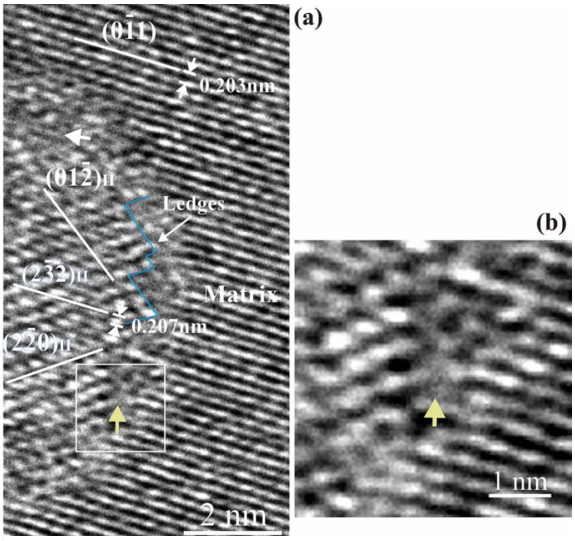

Figure 3 HRTEM image shows the interfacial structure of an ODS nanoparticle in K3. (a) Facets, ledges, and remnant of amorphous domains (marked by arrows) can be found at the oxide (domain II)/matrix interface and (b) a higher magnification view of an amorphous domain in the framed area in **(a)**. *From [14]*

cluster of the oxide material. A discussion of sub-nanometer ODS particles discovered in the as manufactured steels is deferred to section ***6.2***.

6.2 Dual beam experiments with He and Fe ions with TEM PIE

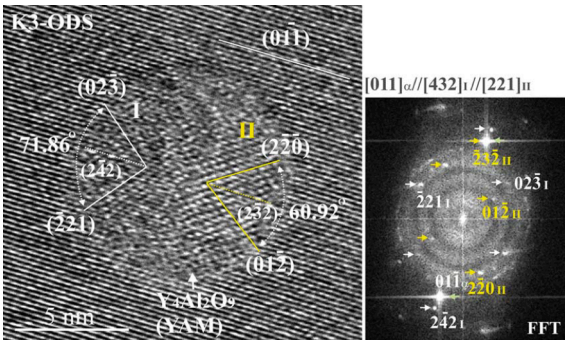

Figure 4 HRTEM image shows the formation of multiple $Y_4Al_2O_9$ domains in an oxide nanoparticle. Two different orientation relationships between $Y_4Al_2O_9$ oxide and the matrix can be readily derived from the FFT image. *From [14]*.

Oxide dispersion strengthened (ODS) steels, which are produced by mechanical alloying (MA) of the elemental, or prealloyed, metallic powder with yttria (Y_2O_3) oxide powder and then consolidated by hot extrusion or hot isostatic pressing, are a class of advanced structural materials with a potential for use at elevated temperatures due to the dispersion of thermally stable oxide nanoparticles into the matrix. ODS steels are resistant to radiation-induced swelling and have improved creep strength and oxidation/corrosion resistance at elevated temperatures compared to conventional steels. Thus an operating temperature of the first wall in future fusion engines of as much as 650°C [6] may be possible.

Structures of nanoparticles in Fe-16Cr-4.5Al-0.3Ti-2W-0.37 Y_2O_3 (K3) and Fe-20Cr-4.5Al-0.34Ti-0.5Y_2O_3 (MA956) oxide dispersion strengthened (ODS) ferritic steels have been studied using high-resolution transmission electron microscopy (HRTEM) techniques to understand the formation mechanism of nanoparticles. The observation of Y-Al-O complex-oxide nanoparticles in both ODS steels imply that decomposition or amorphization of Y_2O_3 in association with internal oxidation of Al occurred during mechanical alloying. While the majority of oxide nanoparticles formed in both steels is $Y_4Al_2O_9$, a few oxide particles of $YAlO_3$ are occasionally also observed. These results reveal that Ti(0.3 wt %) plays an insignificant role in forming oxide nanoparticles in the presence of Al(4.5 wt %). HRTEM observations of crystalline nanoparticles larger than ~2 nm and amorphous or disordered cluster domains smaller than ~2 nm provide an insight into the formation mechanism of oxide nanoparticle in MA/ODS steels, which we believe from our observations involves solid-recrystallization from an amorphous precursor. More details can be found in a

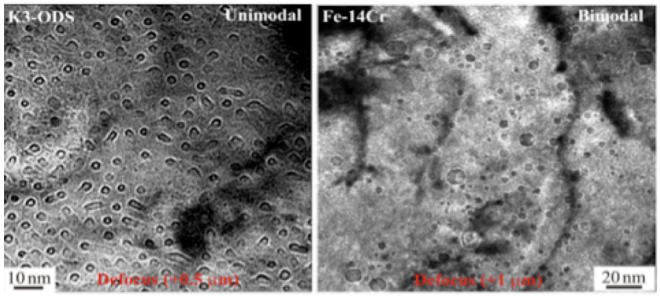

Figure 5 A comparison is shown of a steel with nanoparticles (left) and a steel without nanoparticles (right) both irradiated with Fe and He under the same conditions. The specimen with nanoparticles exhibits small bubbles all below the critical size, and hence no void growth. The specimen without particles shows the start of deleterious void growth. *From (14)*

comprehensive paper published recently [14].

The role of nanoparticles in suppressing radiation-induced swelling is revealed through TEM examinations of cavity distributions in ion-irradiated Fe-14Cr and K3-ODS ferritic steels. HRTEM observations of helium-filled cavities (helium bubbles) preferably trapped at nanoscale oxide particles and clusters in ion irradiated K3-ODS were observed. The difference between the sequestration of He in an ODS alloy and in a ferritic martensitic alloy is shown in Figure 5. This work is described in more detail in our *Phys. Rev.* paper [14].

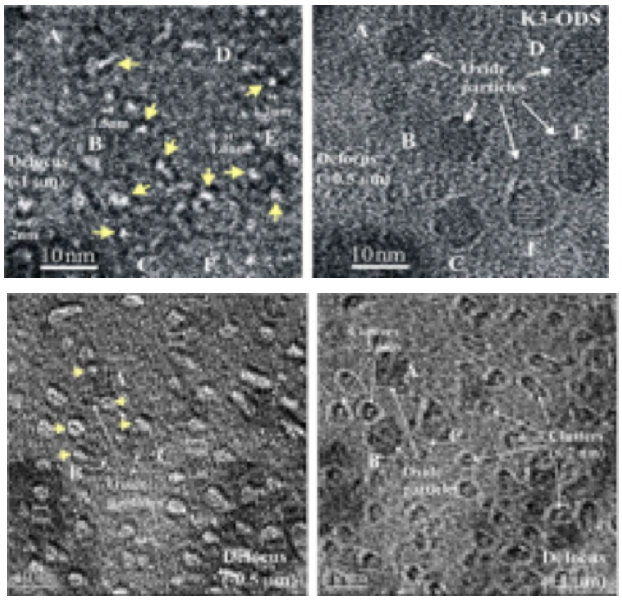

Figure 6 TEM images show *(top)* many spherical cavities (*d*=1–2 nm**)**, which are mostly located at the oxide/matrix interfaces, can be clearly seen in an underfocus condition: −1 μm; the crystalline-oxide particles appeared with lattice fringes **(**labeled A through F; ***d***=5–10 nm**)** can be more readily seen under an overfocus condition of +0.5 μm; *(bottom)* the formation of cavities in association with crystalline-oxide particles **(**labeled A, B, C; *d*≈10 nm**)** and clusters **(***d*<2 nm**)**, both can be more readily seen under an overfocus condition of +0.5 μm. *From [14]*

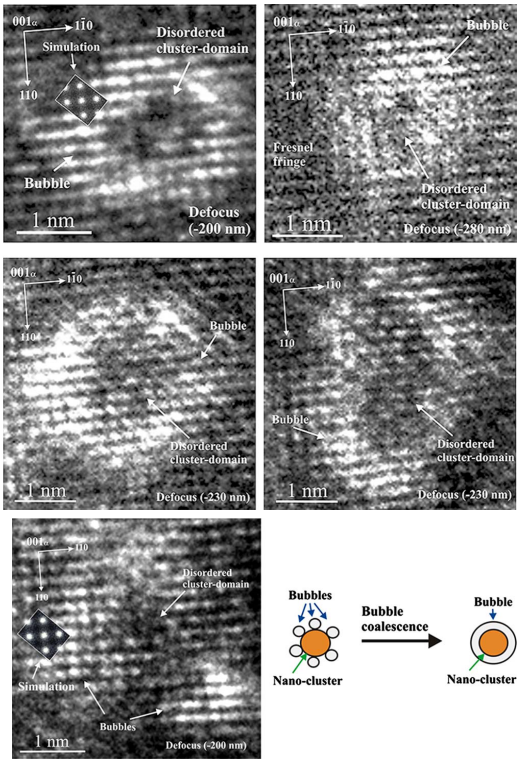

Figure 7 (a) HRTEM images of helium bubbles in association with cluster domains of various shape. Here each helium bubble appears as white contrast surrounded by a dark Fresnel fringe in each underfocused image; (b) HRTEM image shows the trapping of several individual bubbles at a disordered cluster domain, which suggests that the appearance of cluster core/bubble shell is a result of the coalescence of small bubbles as conceptualized in the illustration. *From [14]*

A discovery we made in this work is that sub-nanometer size particles sequester He in such a way as to form He clouds around the particle. Larger particles sequester He by forming small bubbles at the particle matrix interface. This comparison is shown in Figure 6 and Figure 7. It is interesting to note that the sub-nanometer particles were not observable with TEM until they became decorated with He Figure 7. This observation explains why the 3D atom probe technique counts many more particles than TEM observations. The very small particles are actually the dominant source of He sequestration by virtue of their numbers. This suggests that the optimal size distribution for ODS particles is a bimodal one, consisting of sub-nanometer particles for He management and larger (>2 nm) diameter particles for improved high temperature mechanical properties.

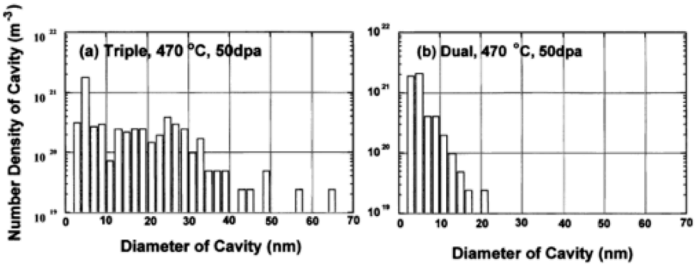

Figure 8 Size distributions of cavities formed in F82H steel irradiated at 470°C to 50 dpa with the triple and dual ion beams under fusion condition. It was measured at depths from 0.9 to 1.1 mm. *From [2]*

6.3 Triple beam experiments with H, He, and Fe ions.

The synergistic aspects of simultaneous implantation of hydrogen along with He and displacement damage have been performed for Fe(Cr) and K3-ODS steel using triple beam irradiation at the CEA-Saclay JANNUS facility. A previously unreported void structure is seen in Fe(Cr) irradiated specimens that may explain the anomalously large swelling seen during triple ion beam irradiations by Tanaka *et al.*,[1].

Wakai and co-workers have addressed the question of anomalous swelling associated with H implantation in triple beam experiments focused on the technically relevant alloy F82H [2,3]. In their two papers they confirmed the synergistic effect reported in [1] for Fe(Cr) model alloys, and have even demonstrated the neutron spectral dependence by varying the H and He to dpa ratio to simulate fusion and spallation conditions at 50 dpa at three temperatures (470, 510 and 600°C) and at 1 μm depth into the

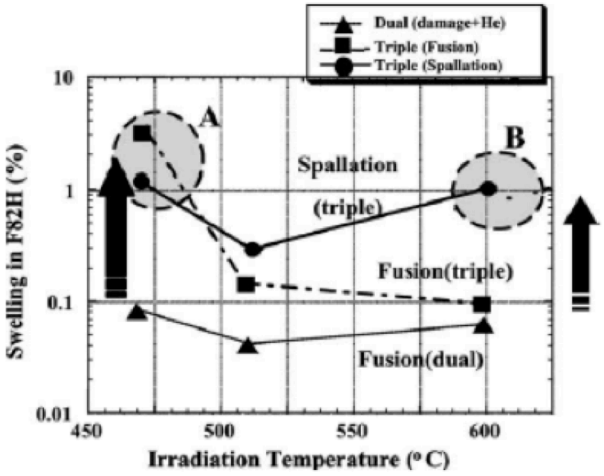

Figure 9 The dependence of swelling of F82H steels on irradiation temperature under these conditions. In the area A the synergistic effect of displacement damage, helium and hydrogen occurred, and in the area B the enhancement of swelling was caused by the synergistic effect of displacement damage and high concentration helium. *From [3]*

specimen. Figure 8 andFigure 9 show a summary of the cavity statistics and the swelling data respectively. The dpa dose of 50 dpa is relevant for what one would want for a DEMO structural. Two very important issues are raised by this work:

1) First is the underlying mechanism resulting in the synergistic effect of hydrogen. Wakai and co-workers measured the hydrogen content of the triple beam irradiated specimens that showed a large synergistic swelling. They report no hydrogen present in the volume of material under test. What this means is that while there is evidence for a synergistic effect from hydrogen the hydrogen itself does not remain in the specimen. One might say that the hydrogen is acting like a catalyst.
2) With this in mind, there is a very important question regarding the reaction kinetics that must be asked. Could the observed synergistic effect be strongly rate dependent in addition to its observed temperature dependence, and can it be expected to greatly diminish or even disappear at the much lower dose rates that would exist in a fusion neutron environment? In addition, one might also ask if there is a peak in the temperature dependence for a given dose rate and spectral condition such as one observes for other swelling phenomena?

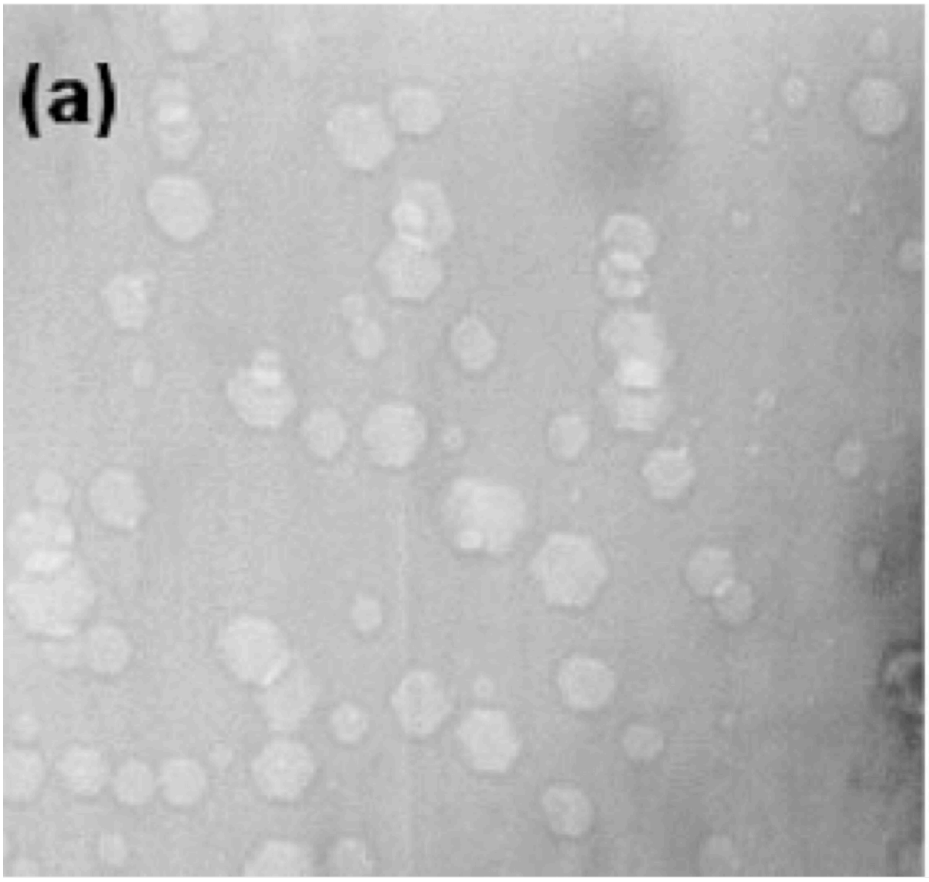

Figure 10 Cavities formed in F82H steel irradiated at 470 _C to 50 dpa at the depth of around 1 mm under (a) triple beams of Fe+, He+ and H+ ions and (b) dual beams of Fe3+ and He+ ions. *From Wakai et al., [3]*

In our first triple beam experiment on Fe(14at%Cr) at 625°C we observed new cavity features that appear to be a consequence of the synergistic effect of hydrogen. We note that the temperature of this triple beam experiment was the same as that used by Tanaka earlier [1]. What is interesting is a comparison of our high resolution images for Fe(14at%Cr) dual and triple beam irradiations at 625°C and 40 dpa with the TEM images shown by Wakai for F82H at 470°C and 50 dpa. This is seen by comparing Figure 10 with Figure 11. We note that both of these are the product of irradiations where synergistically large void swelling is extant. The faceted void-like structures appear to be a common element of the two irradiations, and may hold clues to the kinetics/mechanism for this hydrogen synergistic swelling effect.

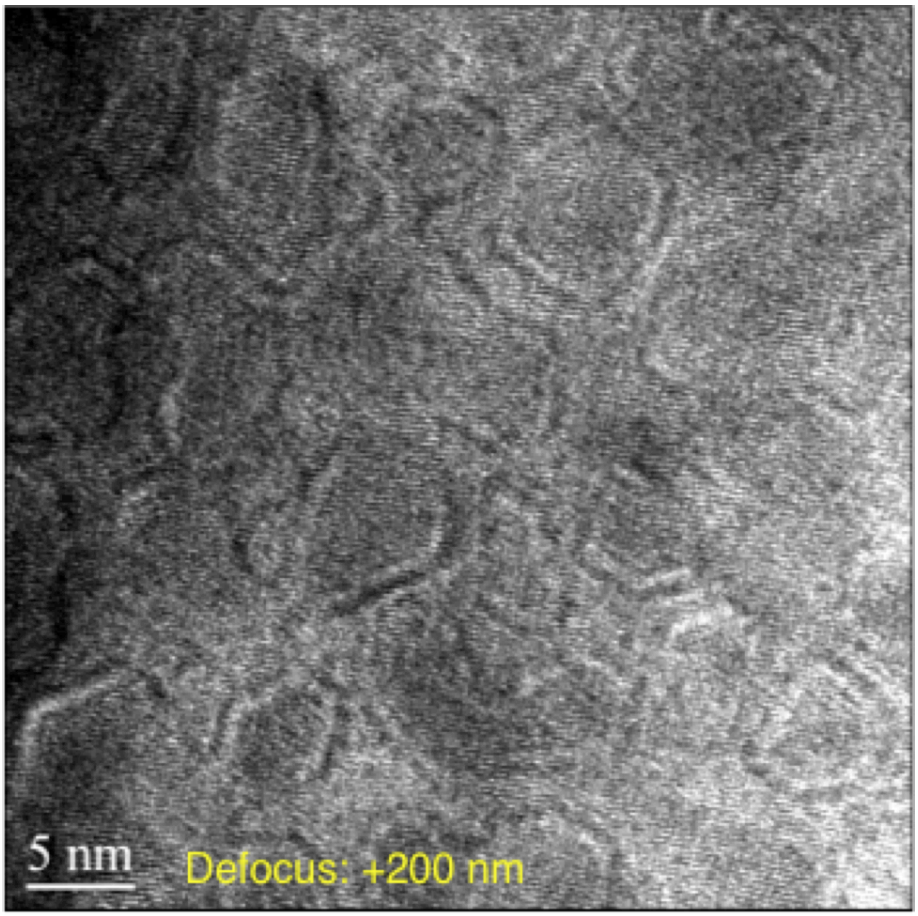

Figure 11 New void like structure is seen in 625°C triple beam irradiation of Fe14Cr, 40dpa, 40 appm H/dpa, and 15 appm He/dpa. Note the similar faceting and large size of the cavities shown to those in Figure 10, both of which are the product of a synergistic hydrogen effect. *P'vt communication: L. Hsiung et. al.,*

6.4 *Theory, simulation, and modeling (TSM)*

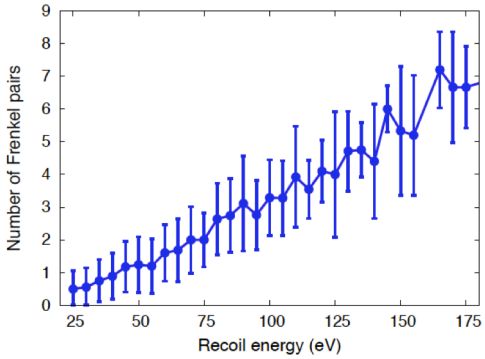

Figure 12 Production of stable Frenkel pairs by He atoms implanted with energies between 0.33 and 4.5 MeV. *P Erhart and J Marian, [15]*

Theiry, simulation, and modeling (TSM) efforts in the last three years have been focused on developing an integrated multiscale methodology to study damage accumulation in *nanostructured* ferritic steels *(nanoparticles dispersed in the matrix)* under fusion irradiation conditions. The behavior of these materials, at relatively high temperatures and neutron doses, is exceedingly complicated, and a comprehensive coverage of all their microstructural features, their coupled behavior, and their evolution with irradiation was simply impractical. Encouraged by the results described above, but constrained by finite resources, we thus chose to select among all the topics of interest, three critical areas of TSM research:

(i) Nature of He ions and α particles upon implantation and transmutation, (respectively).
(ii) Volumetric aspects of metallic oxide particles (ODS-type) on He-atom retention.
(iii) Accumulation of complex irradiation species containing He and H up to high irradiation doses.

The objective was twofold: first, we strived to fill knowledge gaps where the understanding (per the existing literature) was too limited for our purposes; second, the goal was to produce important contributions in terms of high impact papers in the specialized literature. Along the way, our approach was enriched by the concurrent experimental observations taking place and, thus, modified accordingly in a very dynamic and mutually informing fashion.

Regarding (i), the question was the following: when He ions are implanted in a ferritic matrix, are they inserted as substitutional or as interstitial He? The answer is most important due to the enormous difference in mobility between the two species. Interestingly, this question had not been conclusively answered in over three decades of modeling of He effects in steels. As Figure 12 shows, we found that He atoms implanted with energies from 0.33 to 4.5 MeV create their own

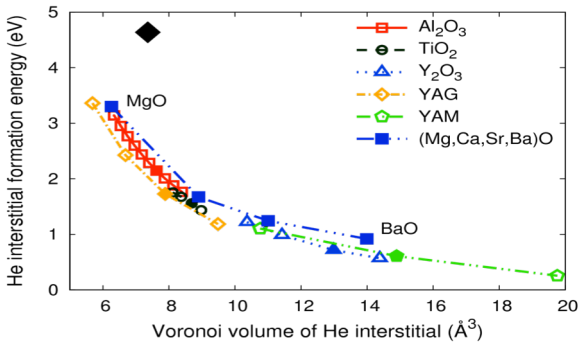

Figure 13 Scaling of the He interstitial formation energy for a number of oxide structures. Yttria substructures produce very low formation energies, which render ODS particles effective thermodynamic volumetric sinks. *P Erhart and J Marian, [16]*

cascade of defects, which may result in correlated recombination of the He atom with a vacancy of its own creation, giving rise to substitutional He [15]. From calculations, we find that up to 3% of all He, either ion implanted or from an (n,α) reaction ends up as substitutional before uncorrelated long-range diffusion occurs. This means that cavity growth can begin almost immediately with these He-vacancy pairs as the seed.

Item (ii) refers to a systematic study of the stability of He atoms within metallic oxide particles (akin to ODS particles) and at their surface. Figure 13 illustrates the formation energy of a He interstitial atom in several oxide structures [16]. The black diamond symbolizes a pure Fe matrix. Clearly, He interstitials will be thermodynamically attracted to oxide particles. In addition, we find that the formation energy scales universally based on the interstitial Voronoi volume of each oxide structure. *Helium formation energies can be predicted across a wide range of oxides based on the volume of the interstitial site.* This "first-of-a-kind" calculation will be very useful to quantify He sequestration at ODS particles.

Finally, (iii) has led to the development of a novel technique never before used for materials science and/or nuclear materials. The so-called *Stochastic Cluster Dynamics* (SCD) method easily permits the treatment of complex species containing more than two types of defects. In addition, by including beneficial aspects of both Monte Carlo and rate theory, our technique lends itself to efficient volume rescaling and long simulated dose periods. Figure 14 shows the first calculations of damage, He, and H accumulation in an Fe(Cr) alloy at 300K up to 50 dpa [17]. The curve shows the formation of He and H bubbles and shows the corresponding incubation doses. We expect SCD to become a leading simulation technique for nuclear materials allowing us to effectively deal with the variations in dpa-dose rate between ion-beam experiments and neutron experiments.

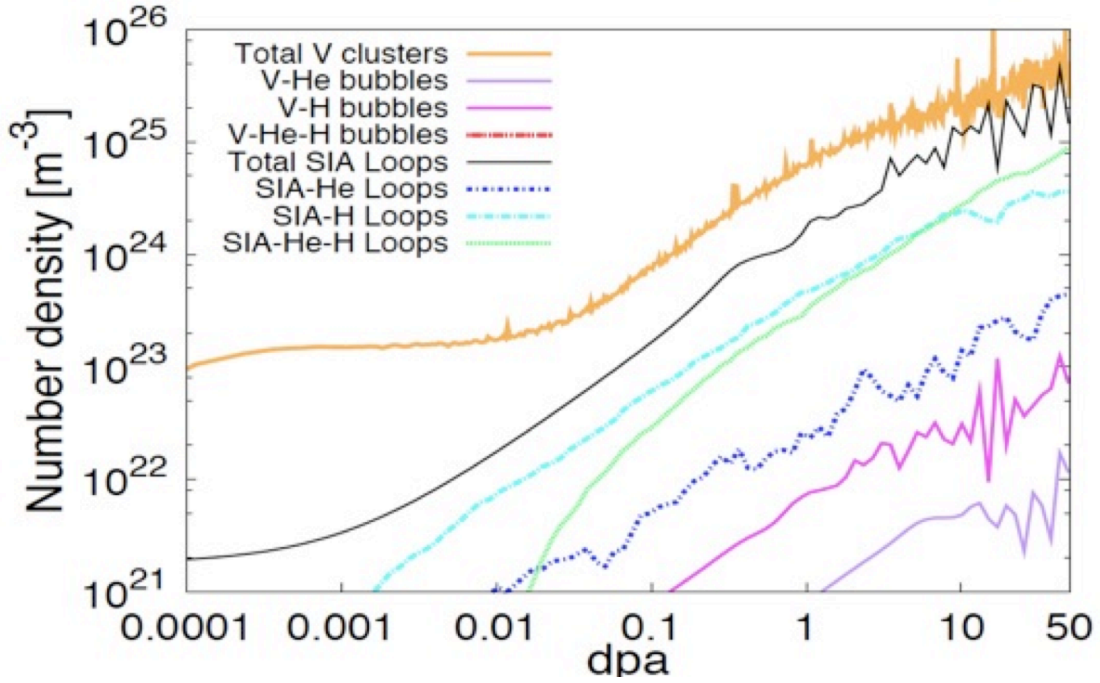

Figure 14 Accumulation of damage in a triple implanted FeCr alloy (Fe, He and H ions). *P'vt comm.,* T. Hoang, J Marian and VV *Bulatov, Also after [17]*

7 Conclusions

The following conclusions were obtained in the work described here:

- ODS particles crystalize during mechanically alloyed powder consolidation and heat treatment from an amorphous precursor.
- ODS particles less than a critical size ~1 nm do not crystalize but they are efficient sequesters of helium
- The critical cavity size for Fe(14%Cr) (d ~2.5 nm) was determined from dual beam irradiations with Fe+He, and is consistent with other measurements using sequential ion beams and neutron irradiations.
- The presence of hydrogen in triple ion beam irradiations of Fe(Cr) alloys and steels leads to anomalously large cavity growth rates but this effect is likely temperature and possibly dose-rate dependent.

8 Recommendations

Multi-ion-beam experiments can emulate the production of displacement damage and the simultaneous production of helium and hydrogen over a broad range of absolute and relative doses. This includes the ability to emulate different neutron spectra by changing the ratio of He and H injected relative to the dpa produced by ballistic collisions. However, because ion beam experiments are performed at dpa rates that are 2 to 3 orders of magnitude greater than those that will be encountered in a fusion environment there remains the reasonable question as regards dose rate effects. While carefully designed triple beam experiments can discover important key mechanisms, such as the anomalously large swelling due to hydrogen synergy [1,2,3], it is not always clear if these mechanisms are relevant to the much lower dose rate (lower dpa rate and lower transmutation rate) encountered in a fusion reactor. For some conditions, particularly where vacancy and interstitials are the only species of interest, it is reasonable to accelerate the interstitial and vacancy transport by raising the temperature to compensate for the higher dpa rate. Invariant equations have been developed for this procedure by Mansur [18] and are often employed to estimate the elevated temperature that will yield the same microstructure in an ion-beam experiment as in a neutron experiment. The introduction of multiple beams, incubation periods, and non-linear changes in the accumulating and changing microstructure make such simple ideas problematic. However, we are not helpless experimentally because we can vary three important parameters in ion-beam irradiation experiments; dose, dose-rate, and temperature. Variations in the evolved microstructure associated with these three variables will lead to improved simulation and modeling because this parametric space will bracket the observed microstructural features. Moreover by exploring this three dimensional space subsequent comparisons with neutron irradiated specimens can be made in such a way as to experimentally determine the invariant set of parameters that yield equivalent microstructural features, or we can expect to eliminate some evolved microstructural features found in ion-beam experiments as irrelevant to the conditions of lower rate neutron irradiations.

1 T. Tanaka, K. Oka, S. Ohnuki, S. Yamashita, T. Suda, S. Watanabe, E. Wakai. J. Nucl. Matl. 329–333 294–298 (2004)(

2 E. Wakai, T. Sawai, K. Furuya, A. Naito, T. Aruga, K. Kikuchi, S. Yamashita, S. Ohnuki, S. Yamamoto, H. Naramoto, S. Jistukawa. J. Nucl. Mater. 307-311 278 (2002)

3 E. Wakai, K. Kikuchi, S. Yamamoto, T. Aruga , M. Ando, H. Tanigawa, T. Taguchi, T. Sawai, K. Oka, S. Ohnuki, Swelling behavior of F82H steel irradiated by triple/dual ion beams, J. Nucl. Mater., 318, 267 (2003)

4 K. Ehrlich, Philos. Trans. R. Soc. London, Ser. A 357, 595(1999).

5 E. E. Bloom, S. J. Zinkle, and F. W. Wiffen, J. Nucl. Mater. 329-333, 12 **(**2004**)**

6 S. Ukai and M. Fujiwara, J. Nucl. Mater. 307-311, 749 (2002)

7 A. Kohyama, M. Seki, K. Abe, T. Muroga, H. Matsui, S. Jitsukawa, and S. Matsuda, J. Nucl. Mater. 283-287, 20 (2000)

8 E. E. Bloom, J. T. Busby, C. E. Duty, P. J. Maziasz, T. E. McGreevy, B. E. Nelson,B. A. Pint, P. F. Tortorelli, and S. J. Zinkle, J. Nucl. Mater. 367-370, 1 **(**2007**)**.

9 J. Boutard, A. Alamo, R. Lindau, and M. Rieth, C. R. Phys. **9**, 287 **(**2008**)**.

10 E. E. Bloom, J. Nucl. Mater. 85-86, 795 (1979)

11 J. F. Ziegler, J. P. Biersack, M.D. Ziegler, SRIM: The stopping and Range of Ions in Matter, Lulu Press Co.; 860 Aviation Parkway; Suite 300; Morrisville, NC, 27560 USA

12 C. Boudias and D. Monceau, The crystallographic software for research and teaching, Senlis, France, 1989–1998.

13 Y. Serruys et al., JANNUS: experimental validation at the scale of atomic modeling, C. R. Physique 9 (2008) 437–444, and Y. Serruys et al., JANNUS: A multi-irradiation platform for experimental validation at the scale of the atomistic modeling, J. Nucl. Mater. **386-388**, , pp 967-970, (30 April 2009)

14 L. Hsiung, M. Fluss, S. Tumey, B. Choi, Y. Surruys, F. Williams, and A. Kimura, "Formation mechanism and the role of nanoparticles in Fe-Cr ODS steels developed for radiation tolerance," Phys. Rev., B 82 p.184130, (2010).

15 P Erhart and J Marian, , "Calculation of the substitutional fraction of ion-implanted He in an Fe target",J. Nucl. Mater. 414, pp. 426-430, (2011).

16 P Erhart and J Marian, "Helium affinity of metallic oxide particles in bcc Fe" in preparation (2011)

17 J. Marian, V. V.Bulatov, "Stochastic Cluster Dynamics Method for Simulations of Multispecies Irradiation Damage Accumulation" J. Nucl. Mater., 415 pp. 84-95, (2011)

18 L.K. Mansur, *J. Nucl. Mater.*, vol. 206, pp. 306–323, (1993).